Unsaturated Linkages in Dioxythiophene−Benzothiadiazole Donor−Acceptor Electrochromic Polymers: The Key Role of Conformational Freedom

Pierre M. Beaujuge,[†] Svetlana V. Vasilyeva,[†] Stefan Ellinger,[†] Tracy D. McCarley,[‡] and John R. Reynolds*,[†]

The George and Josephine Butler Polymer Research Laboratory, Department of Chemistry, Center for Macromolecular Science and Engineering, University of Florida, Gainesville, Florida 32611, and Department of Chemistry, Louisiana State University, Baton Rouge, Louisiana 70803

Received February 6, 2009; Revised Manuscript Received April 7, 2009

ABSTRACT: The perspective of generating new colors commonly difficult to attain such as cyan blue and greens of various tones and saturations has motivated the design of conjugated polymer finely tuned in their molecular structure to reassemble the optical features desired in the context of non-emissive electrochromic device (ECD) applications. Herein, we report on a series of soluble donor−acceptor (DA) conjugated polymers involving 3,4-dioxythiophenes (DOTs) and 2,1,3-benzothiadiazole (BTD) constructed in combination with unsaturated linkages, namely ethynylene and *trans*-ethylene, and compare these to their fully polyheterocyclic DA control analogues with careful emphasis on optical, electrochemical, and electrochromic (EC) properties. As confirmed by spectroelectrochemical analysis, ethynylene linkers hindered the formation of a defined bipolaronic transition in the near-IR and were thus found disruptive with respect to the EC potential of their subsequent alternating copolymers. On the other hand, the presence of *trans*-ethylene spacers incorporated in the DA polymeric backbones allowed further narrowing of the energy gap so that new colors distinct from that exhibited by the control polymers were accessed including saturated green, a complementary color in the realization of polymeric EC displays. Systematic spectroelectrochemical analysis of each novel DA polymer is provided that offers clear evidence of the requirement for conformational freedom and stable quinoidal geometries upon electrochemical oxidation as cathodically coloring electrochromic polymers (ECPs) are switched reversibly to their transmissive doped state.

Introduction

Relying on the concept of energy band broadening induced in a macromolecular conjugated system involving alternating electron-rich and -poor substituents,[1] the donor−acceptor (DA) approach has found its foremost application in the design and synthesis of light-emitting semiconductors[2] and low-bandgap photovoltaics absorbing effectively over the visible spectrum with the goal of improving the solar energy conversion in bulk-heterojunction solar cells.[3,4] Other impacted areas in the expanding field of organic electronics include *n*-channel semiconductors, ambipolar organic thin-film transistors,[5] and chemical biosensors.[6,7] In recent years, the DA approach has also been applied to non-emissive organic electrochromics (EC),[8] opening up new perspectives in extending the palette of colors available[9] needed for EC display technologies. Of particular interest in this area are π-conjugated electrochromic polymers (ECPs) that combine high optical contrasts and long-term redox stability with ease in bandgap/color engineering via structural control as well as mechanical deformability, a requirement for flexible electronic systems.[10−12] Their potential for practical scalability and high-throughput solution processing is an additional major appeal when compared to their inorganic counterparts[12−14] in applications comprising large-area information displays or portable devices made of finely printed pixel arrays. Further, being operational under a wide range of viewing angles and lighting conditions including direct sunlight, low-voltage-driven polymeric ECDs promise to impact the development of reflective and transmissive color-changing systems spanning "smart" polychromic glass technologies[10,15] and e-papers.[16,17]

More than just broadening the range of red and blue ECPs available to the color green, in 2004 Wudl et al. introduced the idea that the DA approach could be judiciously utilized in engineering novel EC systems exhibiting hues and saturations generally difficult to access.[8] Beside its alternating DA structure, the reported electroactive polymeric material was designed with two distinct chromophores in order to exhibit the two-band absorption in the visible desired for a system reflecting/transmitting green light. While its longer wavelength absorption band was found to deplete extensively upon oxidative doping, the optical transition associated with the smaller chromophore (the one in broken conjugation with the main chain) could not be bleached effectively, leaving an oxidized state with remnant color[18] hindering the use of this polymer in colored-to-transmissive switching display devices. The persistent absorption of the doped state remained even after a soluble version of this first promising neutral-state green ECP was achieved.[11,18] It is only recently that a first set of green-to-transmissive ECPs has been reported based on the observation that DA alternating copolymers tend to display two distinct energy transitions[19,20] which can bleach simultaneously on electrochemical oxidation.[21,22] In parallel, neutral state deep-blue PEDOT which switches to a transmissive sky-blue color state is not a solution-processable ECP and is commonly electropolymerized in situ. Further, its near-IR optical transitions overlap with the visible decreasing the transmissivity of the p-doped state considerably in devices. Here, an alternative blue-to-colorless ECP candidate could be found to anticipate the path to commercialization.

Considering the growing interest in solution-processable ECPs, an essential step forward is to develop a better understanding of their fundamental structure−property relationships. To date, few reports address the general characteristics of conjugated polymers suitable for use in EC applications.[12,23,24] Published work often refers to the EC potential of a newly

* Corresponding author. E-mail: reynolds@chem.ufl.edu.
[†] University of Florida.
[‡] Louisiana State University.

10.1021/ma9002787 CCC: $40.75
Published on Web 05/13/2009

Chart 1

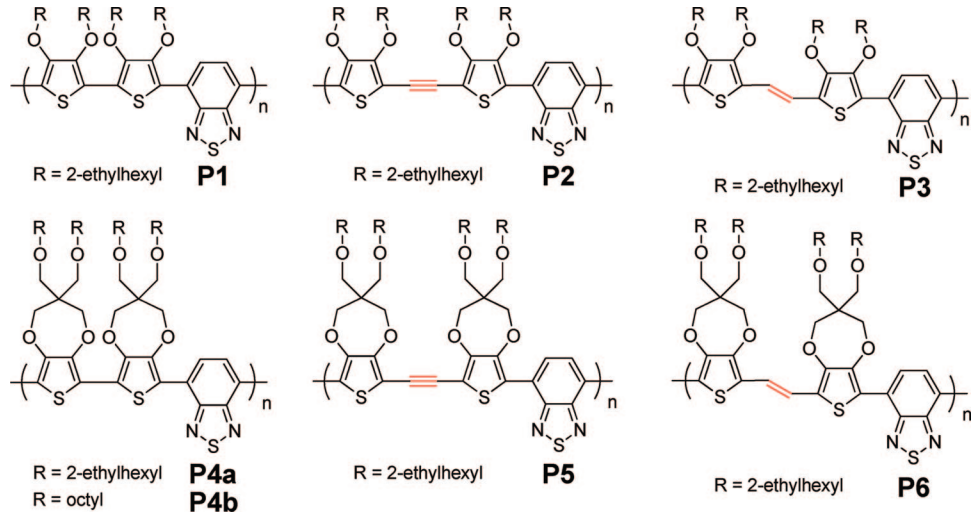

synthesized system without providing any structural reasoning that lead to the desired properties. This lack of systematic structure−property comparisons has motivated us to fill the gap by reporting on a carefully chosen set of conjugated polymers allowing us to establish parallels and trends between molecular structures and EC performance.

In this contribution, we report on the synthesis, electrochemical, and electrochromic performance of a series of alternating conjugated DA polymers containing ethynylene or *trans*-ethylene spacers. The polymers described in Chart 1were achieved with the intention of evaluating the effect of introducing unsaturated linkers in the conjugated backbone of cathodically coloring ECPs. More than just finely tuning the optical properties of the polyheterocyclic DA parent polymers (**P1**, **P4a**, and **P4b**), incorporation of the unsaturated linker could open a pathway toward the synthesis of ECPs made of multiple chromophores randomly copolymerized to give access to any possible hue, including the color black such as desired for electronic ink-based applications.

Experimental Section

Materials and Methods. Tetra-*n*-butylammonium perchlorate (TBAP) was synthesized by the metathesis of tetra-*n*-butylammonium bromide (98%, Sigma-Aldrich) and concentrated perchloric acid (≥69%, Fluka). The product was then recrystallized three times from isopropyl alcohol and dried in a vacuum oven for 3 days. Lithium tetrafluoroborate ($LiBF_4$) (anhydrous, 99.998%, Aldrich) was used as received. The electrolyte salts were stored in an argon-filled drybox. All other reagents and starting materials were purchased from commercial sources and used without further purification, unless otherwise noted. The solvents were distilled and dried using known methods.[25] All reactions were carried under an argon atmosphere unless otherwise mentioned. ^{1}H NMR and ^{13}C NMR spectra were collected on a Mercury 300 MHz using $CDCl_3$ and were referenced to the solvent residual peak ($CDCl_3$: ^{1}H: δ = 7.26 ppm; ^{13}C: δ = 77.23 ppm). High-resolution mass spectrometry was performed by the spectroscopic services at the Department of Chemistry of the University of Florida with a Finnigan MAT 96Q mass spectrometer. MALDI-MS was carried out using a setup previously described.[36] Gel permeation chromatography (GPC) was performed using a Waters Associates GPCV2000 liquid chromatography system with its internal differential refractive index detector (DRI) at 40 °C, using two Waters Styragel HR-5E columns (10 μm PD, 7.8 mm i.d., 300 mm length) with HPLC grade THF as the mobile phase at a flow rate of 1.0 mL/min. Injections were made at 0.05−0.07% w/v sample concentration using a 220.5 μL injection volume. Retention times were calibrated against narrow molecular weight polystyrene standards (Polymer Laboratories, Amherst, MA). Electrochemistry was performed using a single-compartment three-electrode cell with a platinum wire or a Pt flag as the counter electrode, Ag/Ag^+ reference electrode or a silver wire pseudoreference electrode calibrated using a 5 mM solution of Fc/Fc^+ in 0.1 M $LiBF_4$ and TBAP/propylene carbonate (PC) electrolyte solutions, and a platinum disk (0.02 cm^2) or ITO-coated glass slide (7 × 50 × 0.7 mm, sheet resistance, R_s = 8−12 Ω/cm^2) as the working electrode. The ITO electrodes were purchased from Delta Technologies, Ltd. All potentials were reported vs Fc/Fc^+. An EG&G Princeton Applied Research model 273A potentiostat/galvanostat was used under the control of Corrware II software from Scribner and Associates. Electrochemical measurements were carried out in an argon-filled drybox (Vacuum Atmospheres). All absorption spectra including spectroelectrochemistry studies were performed using a Varian Cary 500 Scan UV−vis−near-IR spectrophotometer. Colorimetry measurements were obtained using a Minolta CS-100 Chroma Meter. The sample was illuminated from behind with a D50 (5000K) light source in a light booth designed to exclude external light.

Synthesis of Macromonomers M1, M1′, M2, M2′ and Polymers P1, P4a, P4b. The synthesis of **M1**, **M1′**, **M2**, **M2′**, **P1**, and **P4a** has been previously reported.[13] **P4b** was synthesized using conditions analogous to those described for **P4a**. ^{1}H NMR (300 MHz, $CDCl_3$): δ = 8.34 (bs, 2H), 4.29 (bs, 8H), 3.67 (bs, 8H), 3.47 (bs, 8H), 1.27 (bs, 36H), 0.86 (bs, 24H).

Synthesis of Polymer P2. Macromonomer **M1′** (245 mg, 0.252 mmol), 1,2-bis(trimethylstannyl)ethyne (88.7 mg, 0.252 mmol), and tetrakis(triphenylphosphine)palladium (4 mol %) were purged with argon/vacuum (3 times) and subsequently dissolved in a mixture of dry toluene (8 mL) and degassed anhydrous dimethylformamide (1.5 mL). The solution was heated to 100 °C. After 72 h, the reaction mixture was cooled to room temperature and poured into methanol-deionized water (2:1, 200 mL). The precipitate was filtered through a Soxhlet thimble, purified via Soxhlet extraction for 12 h with methanol, and extracted for 2 h with chloroform. The chloroform fraction was concentrated by evaporation, and the polymer was precipitated into deionized water, collected as a dark solid, and dried under vacuum overnight (81%). ^{1}H NMR (300 MHz, $CDCl_3$): δ = 8.47 (bs, 2H), 7.72 (m, chain ends), 7.41 (m, chain ends), 4.1−3.9 (br, 8H), 1.8−1.2 (br, 36H), 1.1−0.6 (br, 24H).

Synthesis of Polymer P5. Macromonomer **M2′** (245 mg, 0.209 mmol), 1,2-bis(trimethylstannyl)ethyne (73.5 mg, 0.209 mmol), and tetrakis(triphenylphosphine)palladium (4 mol %) were purged with argon/vacuum (3 times) and subsequently dissolved in a mixture of dry toluene (8 mL) and degassed anhydrous dimethylformamide (1.5 mL). The solution was heated to 100 °C. After 72 h, the reaction mixture was cooled to room temperature and poured into methanol-deionized water (2:1, 200 mL). The precipitate was filtered through a Soxhlet thimble, purified via Soxhlet extraction for 12 h with methanol, and extracted for 2 h with chloroform.

Scheme 1

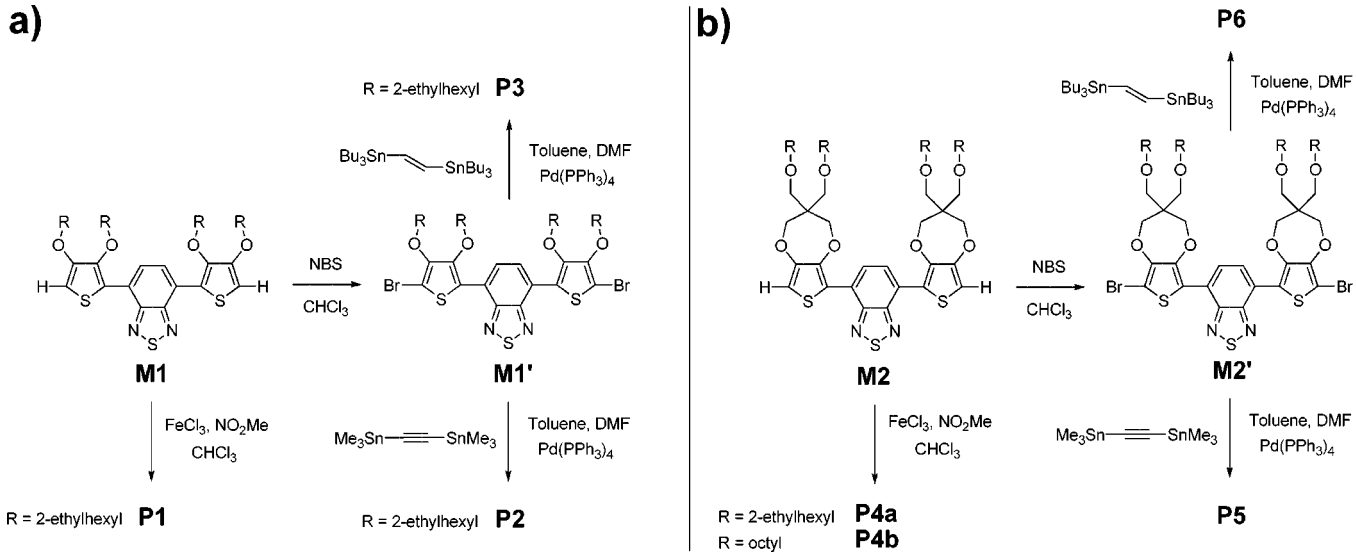

The chloroform fraction was concentrated by evaporation, and the polymer was precipitated into deionized water, collected as a dark solid, and dried under vacuum overnight (72%). ^{1}H NMR (300 MHz, $CDCl_3$): δ = 8.29 (bs, 2H), 7.72 (m, chain ends), 7.41 (m, chain ends), 4.20 (bs, 8H), 3.58 (bs, 8H), 3.32 (bs, 8H), 1.28 (bs, 36H), 0.89 (bs, 24H).

Synthesis of Polymer P3. Macromonomer **M1′** (315 mg, 0.324 mmol), 1,2-bis(tributylstannyl)ethene (196.6 mg, 0.324 mmol), and tetrakis(triphenylphosphine)palladium (4 mol %) were purged with argon/vacuum (3 times) and subsequently dissolved in a mixture of dry toluene (15 mL) and degassed anhydrous dimethylformamide (3 mL). The solution was heated to 100 °C. After 72 h, the reaction mixture was cooled to room temperature and poured into methanol−deionized water (2:1, 200 mL). The precipitate was filtered through a Soxhlet thimble, purified via Soxhlet extraction for 12 h with methanol, and extracted for 2 h with chloroform. The chloroform fraction was concentrated by evaporation, and the polymer was precipitated into methanol−deionized water (1:1, 100 mL), collected as a dark solid, and dried under vacuum overnight (70%). ^{1}H NMR (300 MHz, $CDCl_3$): δ = 8.41 (bs, 2H), 7.72 (m, chain ends), 7.41 (m, chain ends), 4.1−3.9 (br, 8H), 1.8−1.2 (br, 36H), 1.1−0.6 (br, 24H).

Synthesis of Polymer P6. Macromonomer **M2′** (300 mg, 0.256 mmol), 1,2-bis(tributylstannyl)ethene (155.2 mg, 0.256 mmol), and tetrakis(triphenylphosphine)palladium (4 mol %) were purged with argon/vacuum (3 times) and subsequently dissolved in a mixture of dry toluene (15 mL) and degassed anhydrous dimethylformamide (3 mL). The solution was heated to 100 °C. After 72 h, the reaction mixture was cooled to room temperature and poured into methanol−deionized water (2:1, 200 mL). The precipitate was filtered through a Soxhlet thimble, purified via Soxhlet extraction for 12 h with methanol, and extracted for 2 h with chloroform. The chloroform fraction was concentrated by evaporation, and the polymer was precipitated into methanol−deionized water (1:1, 100 mL), collected as a dark solid, and dried under vacuum overnight (78%). ^{1}H NMR (300 MHz, $CDCl_3$): δ = 8.42 (bs, 2H), 7.72 (m, chain ends), 7.41 (m, chain ends), 4.25 (bs, 8H), 3.60 (bs, 8H), 3.35 (bs, 8H), 1.31 (bs, 36H), 0.91 (bs, 24H).

Results and Discussion

Polymer Synthesis. The fully heterocyclic parent polymers **P1**, **P4a**, and **P4b** were synthesized from the low oxidation potential macromonomers **M1** and **M2** using the mild oxidizing agent $FeCl_3$ and hydrazine as the reducing agent (see Chart 1 and Scheme 1). Details concerning the experimental conditions employed in the synthesis of **M1**, **M2**, **P1**, **P4a**, and **P4b** can be found in previously reported work from our group.[13]

The unsaturated spacer-containing polymers **P2**, **P3**, **P5**, and **P6** were accessed from the halogenated analogues of **M1** and **M2**, namely **M1′** and **M2′**, using traditional Stille polymerization conditions[26] between the tin-functionalized unsaturated linkers and the macromonomers (see Scheme 1). Refluxing mixtures of toluene and dimethylformamide (DMF) were found suitable in the case of these condensations between the bulky, sterically hindered heterocyclic macromonomers and their ethylenic/ethynylenic comonomers, conversely small in size, hence relatively prone to transmetalation mechanisms.

Polymer Characterization. The repeat unit structures of all polymers are supported by ^{1}H NMR (see Experimental Section) and matrix-assisted laser desorption/ionization mass spectrometry (MALDI-MS). Figure 1 shows the MALDI mass spectra of **P1**, **P4a**, **P3**, and **P6** as representative examples.

Using tertiophene[27,28] or *trans*-2-[3-(4-*tert*-butylphenyl)-2-methyl-2-propenylidene]malononitrile (DCTB)[29] as the matrix, ions with masses up to nearly 9000, 12 000, and 20 000 amu were respectively detected for the control polymers **P1**, **P4a**, and **P4b**. As illustrated in Figure 1a, the mass spectrum of **P1** shows an ion series with a spacing of ∼1622 amu between each ion, corresponding to the calculated mass of two repeat units (i.e., one oxidative condensation). Each major ion detected consists of an odd number of repeat units (n = 3, 5, 7, 9) terminated by two chlorines. End-capping via chlorine atoms is not unusual during $FeCl_3$-assisted oxidative polymerizations and has been demonstrated in previous work from McCarley et al.[27] In Figure 1b, **P4a** is represented by very intense peaks at m/z 3037 and m/z 3107, which correspond respectively to trimeric chains possessing H/H and Cl/Cl end groups. The peak at m/z 3107 is part of an ion series with intervals matching the mass of the polymer repeat unit (∼1011 amu). This series ranges from m/z 3000 up to m/z 12 000 (n = 3−12), thereby supporting the presence of a higher molecular weight fraction. In the case of **P4b**, at least two ion series spanning from m/z 3000 to 20 000 (n = 3−19) with ions separated by the mass of the polymer repeat unit (∼1011 amu) were identified. Similarly to **P1** and **P4a**, the dominant series is consistent with oligomers end-capped by chlorine atoms.

The unsaturated linker-containing DA polymers **P2**, **P3**, **P5**, and **P6** were investigated employing DCTB as a matrix. Both the structures of ethynylene-linked **P2** and **P5** were supported by series of ions (n = 1−5 and n = 1, 2) with spacing matching the mass of the repeat unit of the polymers, ∼835 and ∼1036 amu, respectively. The residual masses of these series indicate

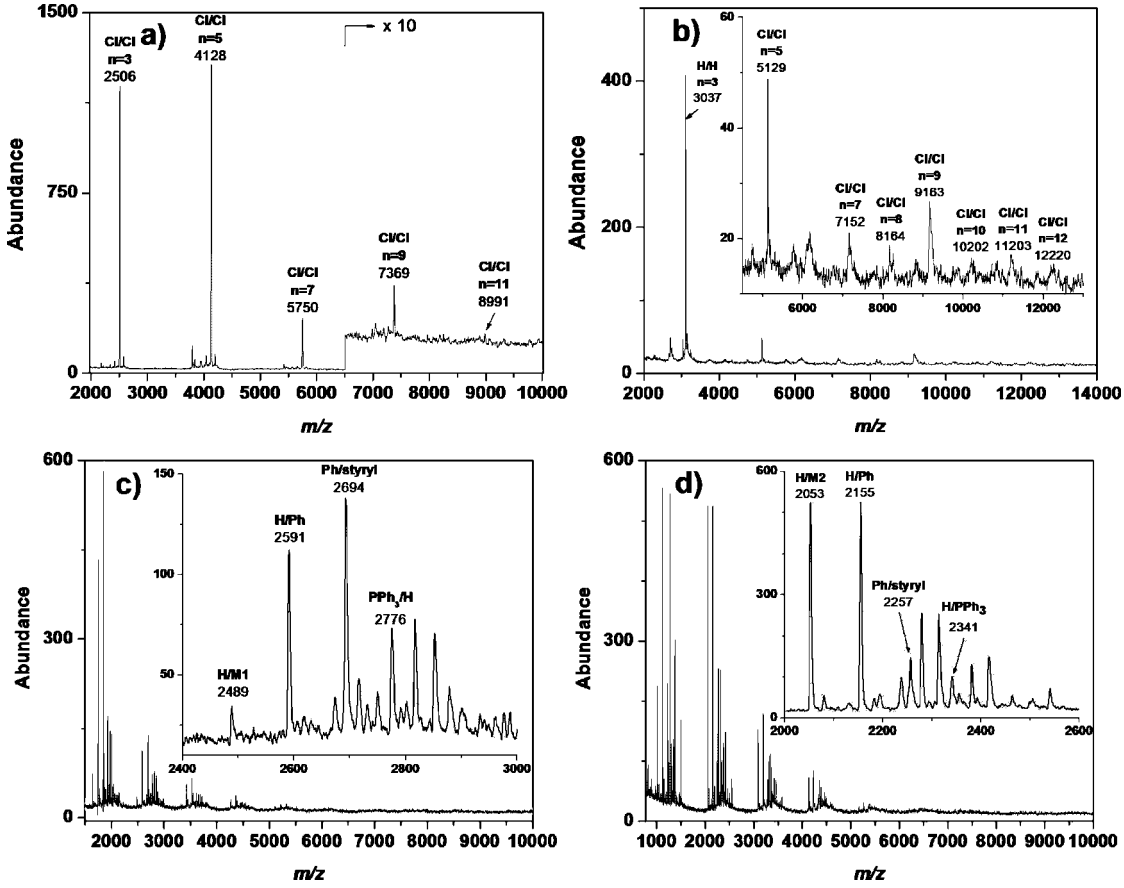

Figure 1. MALDI-MS of DA copolymers (a) **P1**, (b) **P4a**, (c) **P3**, and (d) **P6**. DCTB was used as the matrix in each case.

Table 1. GPC Estimated Weight-Average Molecular Weights of the Copolymers P1, P2, P3, P4a, P4b, P5, and P6 (from THF) and Their Local Absorption Maxima (Solution and Solid State)

					λ_{abs} (nm) in toluene		λ_{abs} (nm) thin film		
polymer	M_w (g mol^{-1})	PDI	av no. of repeat units	av no. of rings	**1**	**2**	**1**	**2**	T_d (°C)[b]
P1	42 700	2.6	20	60	391	638	399	653 (708)[a]	321
P2	11 800	1.8	7	21	362	553	373	577	213
P3	13 000	1.7	9	27	401	625	416	648 (706)[a]	265
P4a	59 000	2.1	27	81	402	674	408	677 (722)[a]	350
P4b	32 100	2.2	15	45	405	678	407	685	348
P5	16 800	1.9	8	24	346	578	357	578	201
P6	15 500	1.8	9	27	419	677	433	685 (745)[a]	200

[a] Shoulder. [b] Onset decomposition temperature measured by TGA under nitrogen.

that the end groups consist of a hydrogen and an additional monomer unit **M1** (in the case of **P2**) or **M2** (in the case of **P5**) (see Scheme 1) which can be end-capped with a phenylphosphine-derivatized moiety as reported in several other studies.[30] In addition, both of these series have related, lower-intensity series in which a bromine is substituted for the hydrogen end group.

A large number of ion series were detected in the range *m*/*z* 1000−9000 for both **P3** and **P6**, as illustrated in Figure 1c,d. Each series exhibited a spacing of ∼837 amu for **P3** and ∼1038 amu in the case of **P6** matching the masses of the expected repeat units. Residual masses of some of the ion series suggest end groups of hydrogen and phenyl or phenyl and styryl, an experimental observation supported by work from Janssen et al. for instance.[31] Other ion series appear to have end groups of hydrogen and phenylphosphine analogue moieties or hydrogen and an extra aromatic building block **M1** (in the case of **P3**) or **M2** (in the case of **P6**) (see Scheme 1).

It is worth noting that ion series detected in MALDI-MS analyses of polymers commonly occur at much lower masses than those estimated employing conventional gel permeation chromatography (GPC). In fact, discrimination of the higher mass ions take place both during ionization and detection, and the phenomenon is amplified with increasing polymer polydispersity.[32−35]

Molecular weights were further investigated via polystyrene-calibrated GPC employing tetrahydrofuran (THF) as the mobile phase. As illustrated in Table 1, polymers with weight-average molecular weight (M_w) ranging from 11 000 to 60 000 g mol^{-1} with relatively narrow PDIs (1.7−2.6) and number-average molecular weight (M_n) values up to 28 000 g mol^{-1} for the oxidatively polymerized analogues were estimated. Importantly, all polymers had a minimum average number of repeat units of 7 corresponding to a backbone of about 28 unsaturated building units (including heterocycles and unsaturated linkages), which is nearly twice as much as the value at which the electronic properties of conjugated polymers commonly saturate (∼15 aromatic rings).[36] The highest average numbers of unsaturated building units incorporated into a single polymer chain (∼45, 60, and 81) were obtained upon using oxidative polymerization conditions (in synthesizing **P4b**, **P1**, and **P4a**, respectively).

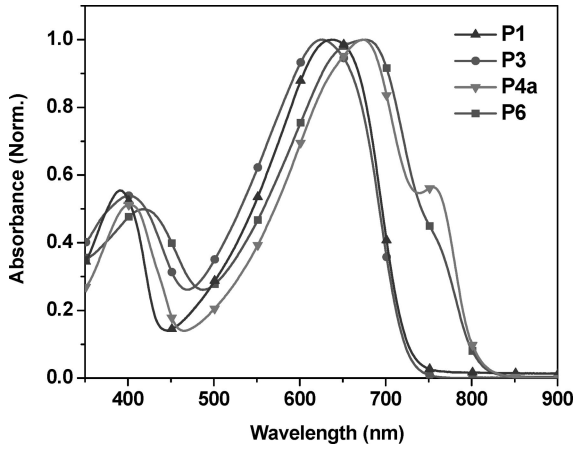

Figure 2. Solution optical absorbance of *trans*-ethylene unsaturated DA copolymers **P3** and **P6** compared to their ethylhexyl-substituted parent copolymers **P1** and **P4a**, respectively, in toluene. The spectrum of each system is normalized at the longer wavelength absorption maximum.

Thermogravimetric analysis in a nitrogen atmosphere of the all-heterocyclic analogues **P1**, **P4a**, and **P4b** revealed only negligible weight loss below 320 °C, demonstrating their high thermal stability. On the other hand, the polymers containing unsaturated linkages exhibited only limited thermal stability in general with clear signs of degradation starting at 200 °C in the case of **P5** and **P6** for instance.

Polymer Solution Optical Absorption. The polymer's maxima of optical absorption in toluene solution are reported in Table 1. All polymers exhibit a two-band absorption in the UV−vis spectral range with a peak-to-peak distance larger than 190 nm, opening a gap of low optical density in the blue, blue-green, or green region. While the lower energy transition can be attributed to the intramolecular donor−acceptor interaction arising from the bonding of electron-rich (DOTs and unsaturated linkages) and electron-deficient (BTDs) building units, the higher energy transition can be assigned to the electron-rich portion of the alternating polymer backbone.[13] As can be seen from the higher energy absorption maxima of **P3** and **P6** relative to **P1** and **P4a** in Figure 2, the insertion of an ethylene spacer between the two electron-donating substituents of these donor−acceptor systems induces a bathochromic shift which also moves the absorption gap from the blue or blue-green to the blue-green or green regions of the visible, hence predicting some significant differences in neutral state colors. To a lesser extent, the high wavelength optical transitions also shift toward longer wavelengths although the onsets of absorption remain nearly identical here in solution and in spite of the spacer insertion. It is expected to see a further bathochromic shift as we examine thin films where the degree of coplanarity of the polymer main chains influences the optical bandgap. We attribute the shoulders tailing between 750 and 800 nm in the case of **P4a** and **P6** to the aggregation of the highest molecular weight fraction of the polymers in solution (although no visible aggregation could be perceived) as elevating the temperature of the polymer/toluene solutions had the effect of reducing their intensity.

Polymer Electrochemistry. The redox properties of all polymers were investigated via cyclic voltammetry (CV) and differential pulse voltammetry (DPV) with the goal of determining how polymer oxidation/reduction potentials, associated HOMO/LUMO energy levels, and relative electrochemical bandgaps vary as a function of the structural modifications. In comparison to CV, DPV offers a higher sensitivity and sharper redox onsets throughout the electrochemical process owing to a reduced contribution of the charging background currents which, in turn, enhances the accuracy and reliability of the bandgaps estimated electrochemically. Thin films of the polymers were drop-cast onto platinum disk electrodes from toluene solutions (6 mg mL^{-1}) for characterization in an argon-filled drybox. A platinum flag was used as the counter electrode in combination with a Ag/Ag^+ reference electrode, and all results were subsequently calibrated to Fc/Fc^+ (for consistency with the rest of this article). In Table 2, the corresponding polymer energy levels (HOMO and LUMO) are given relative to the vacuum level, considering that the SCE is 4.7 eV vs vacuum[37] and Fc/Fc^+ is 0.38 eV vs SCE,[39] i.e., ∼5.1 eV relative to vacuum.

Prior to characterization, the polymer films were cycled at a scan rate of 50 mV s^{-1} between −0.2 and 0.9 V until they reached a stable and reproducible electrochemical response.[3] The polymer films were found stable to p-type doping during extensive cycling from −0.2 to 0.9 V retaining 90% of their peak currents after 100 switches with the exception of polymers **P2** and **P5**. We attribute the more rapid loss of electroactivity of **P2** and **P5** to the sensitivity of the ethynylene spacers to overoxidation side reactions. In general, the polymers were found to be less stable to n-doping processes.

In 0.1 M $LiBF_4$/propylene carbonate (PC) and 0.1 M TBAP/PC electrolyte solutions, both CV and DPV experiments show similar and reproducible redox behavior for each polymer upon oxidation and subsequent neutralization. However, we found that upon reduction of the polymer films the current responses could only be observed when using TBAP supporting electrolyte. It is worth noting that such specificity to the positively charged balancing counterion has already been reported in the case of various conjugated polymers.[39,40] In fact, during the reduction process, hard electrophilic cations such as lithium induce only minimal conductivity due to "pinning" of the doped state and insufficient delocalization of the charge carrier along the polymer main chain.[41,42]

For consistency, the electrochemical results summarized in Table 2 refer to measurements collected in 0.1 M TBAP/PC solution electrolyte. Careful examination of the data presented in this table highlights the correlations between polymer architecture and electrochemical properties.

For example, the CVs of polymer **P4b** (possessing linear octyl solubilizing side chains) and its branched analogue **P4a** (possessing 2-ethylhexyl substitutents instead) illustrated in Figure 3a show a more reversible redox process with potential peak difference (ΔE_p) of 150 mV in the case of **P4a** while **P4b** has a significantly broader current response of ca. 260 mV. The increase of interchain spacing resulting from the branched nature of the alkyl chains of **P4a** could promote the insertion of charge-compensating ion and lead to a faster redox response (this hypothesis will also be backed up throughout the next sections of this article). However, **P4b** shows a lower electrochemical bandgap as compared to **P4a** probably due to its more extended conjugation in the solid state when compared to that of the branched derivative which is also likely more disordered.[43]

When comparing the dialkoxythiophene (DalkOT)-derivatized polymers **P1**, **P2**, and **P3** with their propylenedioxythiophene (ProDOT) analogues **P4a**, **P5**, and **P6**, respectively, a clear trend is observed in terms of oxidation potential. Upon replacing the DalkOT units with the more electron-rich ProDOTs, lower onsets of oxidation are obtained which result in higher HOMO level estimated values and lower electrochemical bandgaps. Figure 3b shows the DPVs of **P1** (a DalkOT-based derivative) and **P4a** (ProDOT-based) using a step time of 0.1 s, a step size of 2 mV, and an amplitude of 100 mV. **P4a** has an oxidation onset 350 mV less positive and a reduction onset only 120 mV more negative than **P1**. Such a drastic increase of the HOMO

Table 2. Electrochemically Determined HOMO and LUMO Levels, Electrochemical Bandgaps, and Comparison with their Optically Estimated Values for the Copolymers P1, P2, P3, P4a, P4b, P5, and P6[a]

	E_{ox} onset (V)		HOMO (eV)		E_{red} onset (V)		LUMO (eV)		E_{gap} (V)		E_{gap} (V)
polymer	CV	DPV	CV	DPV	CV	DPV	CV	DPV	CV	DPV	optical
P1	0.25	0.25	5.35	5.35	−1.57	−1.52	3.53	3.59	1.82	1.77	1.6
P2	0.51	0.4	5.61	5.5	−1.33	−1.38	3.77	3.72	1.84	1.78	1.75
P3	0.12	0.14	5.22	5.24	−1.46	−1.51	3.54	3.59	1.58	1.65	1.6
P4a	−0.06	−0.1	5.04	5.0	−1.7	−1.64	3.4	3.46	1.64	1.54	1.54
P4b	0.0	0.02	5.1	5.12	−1.6	−1.57	3.48	3.49	1.6	1.59	1.52
P5	0.21	0.24	5.31	5.34	−1.48	−1.47	3.62	3.63	1.69	1.71	1.65
P6	0.07	0.0	5.17	5.1	−1.56	−1.5	3.54	3.6	1.63	1.5	1.5

[a] Oxidation (E_{ox} onset) and reduction (E_{red} onset) potentials are reported vs Fc/Fc^+. HOMO and LUMO energy levels are derived from the electrochemical data (E_{ox} onset and E_{red} onset, respectively) considering that the SCE is 4.7 eV vs vacuum[37] and Fc/Fc^+ is 0.38 eV vs SCE,[38] i.e., 5.1 eV relative to vacuum.

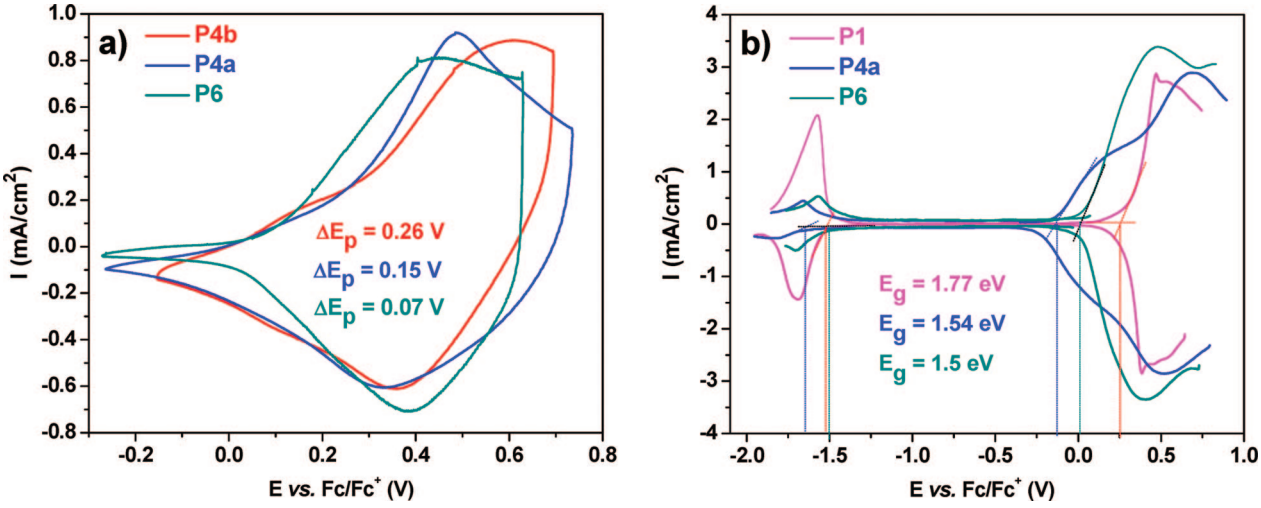

Figure 3. (a) Cyclic voltammograms of **P4a**, **P4b**, and **P6** drop-cast onto platinum disk electrodes (0.02 cm^2) in 0.1 M TBAP/PC electrolyte solution, using a scan rate of 50 mV/s. (b) Differential pulse voltammetry of **P1**, **P4a**, and **P6** drop-cast onto platinum disk electrodes (0.02 cm^2) in 0.1 M TBAP/PC electrolyte solution using a step time of 0.1 s, a step size of 2 mV, and an amplitude of 100 mV.

energy in the case of **P4a** leads to a lower magnitude of the DPV estimated band gap (1.54 eV compared to 1.77 eV for **P1**).

P2 and **P5** contain ethynylene linkages which reduce the degree of conjugation of the subsequent donor−acceptor systems. This effect appears to be the most significant in the case of the less electron-rich DalkOT-derivatized polymer **P2**. Thus, after only several cycles, **P2** loses its electroactivity as CV and DPV current responses become indiscernible from background currents, though a visible thin polymer film (now insulating) is still present at the electrode surface.

The DPV of **P6** is also shown in Figure 3b in order to be compared to that of **P4a**. The observed differences that relate to the electrochemical properties of these polymers, such as a decreased amplitude of the bandgap and a more reversible redox switching in the case of **P6** (ΔE_p(**P6**) = 70 mV and ΔE_p(**P4a**) = 150 mV), can be rationalized by considering the enhanced planarity and extended conjugation length of the **P6** backbone in which a *trans*-ethylene linkage was inserted between the donor−acceptor−donor building blocks. **P1** and **P3** exhibit similar variations in their redox properties, though the differences appear less pronounced.

Expectedly, **P1**−**P6** showed a relatively unstable redox cycle upon n-doping, with **P1** undergoing about 20% loss in cathodic peak current density after 20 cycles, for example. The other polymers were less stable, with 35−50% loss in peak current density after only 5 cycles.

In general, the electrochemically determined bandgaps were found to be slightly larger than the optically estimated values but remain in good agreement.

Polymer Spectroelectrochemistry. Figure 4 uses spectroelectrochemistry to illustrate the propensity of each of the DA polymers to form positively charged carriers upon electrochemical oxidation (p-type doping).

On a practical level, spectroelectrochemical experiments allow probing of redox-induced color/contrast changes. Generally, electrochemical doping induces the formation of radical cations (polarons) and further dications (bipolarons) possessing longer wavelength optical absorption bands than the ones associated with the neutral polymer. The extent of depletion of the neutral state interband transition(s) depends on the degree of stability attained by the charge carriers and the ability of the polymeric backbone to attain its quinoidal geometry (relating to the formation of the bipolaronic states). As a result, substantial variations in electrochromic performance, including neutral state color and switching ability, can be induced with minimal structural changes in the polymer backbone. When the neutral polymer's light absorption is fully transferred from the visible region into the near-infrared (near-IR) upon oxidation, the material is cathodically coloring and yields a highly transmissive doped state. Colored-to-transmissive ECPs are especially useful for integration in "smart" glass technologies and display applications.

All DA polymers were spray-cast from toluene (4−6 mg mL^{-1}) onto indium tin oxide (ITO)-coated glass slides at room temperature. Electrochemical oxidation of the films was carried out in 0.1 M $LiBF_4$/propylene carbonate supporting electrolyte using a silver wire as a quasi-reference electrode (calibrated against Fc/Fc^+) and a platinum wire as the counter electrode.

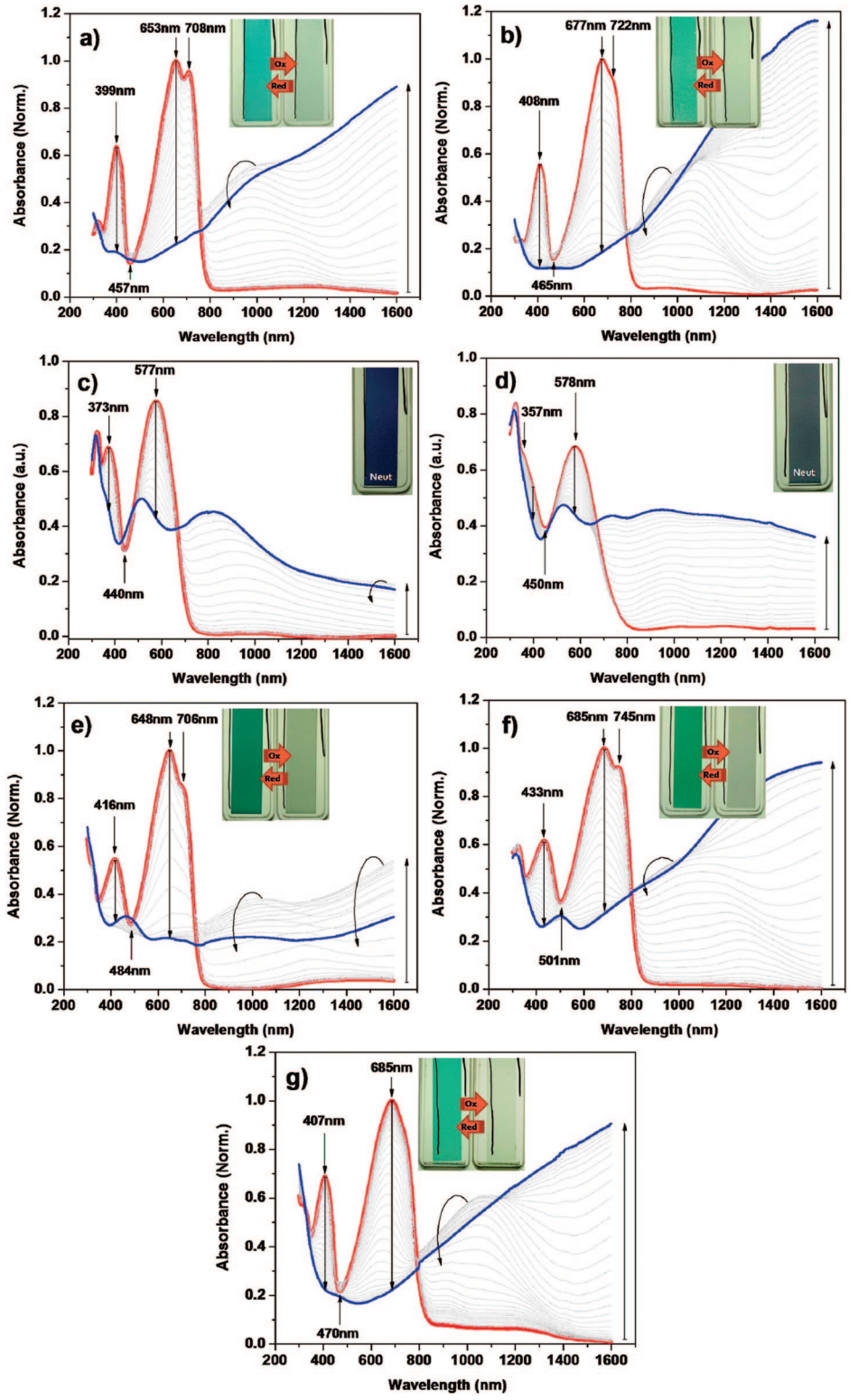

Figure 4. Spectroelectrochemistry of DA copolymer (a) **P1**, (b) **P4a**, (c) **P2**, (d) **P5**, (e) **P3**, (f) **P6**, and (g) **P4b** (spectra a, b, e, f, and g) are normalized at the polymer longer wavelength absorption maximum). Films were spray-cast onto ITO-coated glass from toluene solutions (~4 mg mL^{-1}). Electrochemical oxidation of the films was carried out in 0.1 M $LiBF_4$/PC supporting electrolyte using a silver wire as a quasi-reference electrode (calibrated against Fc/Fc^+) and a platinum wire as the counter electrode. The applied potential was increased (a) in 25 mV steps from +0.3 to +0.5 V and in 10 mV steps from +0.5 to +0.76 V, (b) in 25 mV steps from −0.05 to +0.7 V, (c) in 50 mV steps from −0.17 to +0.23 V and in 25 mV steps from +0.23 to +0.8 V, (d) in 25 mV steps from +0.23 to +0.7 V, (e) in 25 mV steps from +0.33 to +0.73 V, (f) in 25 mV steps from +0.2 to +0.83 V, and (g) in 25 mV steps from +0.17 to +0.72 V.

Figure 4a,b shows the spectral changes occurring in the 300−1600 nm range upon electrochemical oxidation of **P1** and **P4a** which both exhibit a two-band absorption in the visible spectrum with a major contribution from the lower energy transition attributed to the intramolecular donor−acceptor electronic interaction. With an open gap in light absorption in the range 455−470 nm, coupled to a moderate absorption between 350 and 450 nm and a broad coverage of the red portion of the visible, these polymers exhibit different hues of blue. While **P1** shows a deep cyan blue neutral state, **P4a** is blue-

green due to the more red-shifted low-energy transition, allowing a minor green transmission. The spectral differences observed in their neutral state, along with the estimated variation of 0.06 eV in optical bandgaps (calculated from the onset of their longer wavelength absorption band), relate to the difference in molecular orbital energy levels with ProDOT bringing a higher energy HOMO to the donor−acceptor conjugated system. Oxidation of the films induces simultaneous and extensive bleaching of both the short and long wavelength absorption bands. Taking the two local absorption maxima as references, **P1** shows a transmittance change ($\Delta\%T$) of 41.7% (λ_{abs1}) and 50.3% (λ_{abs2}) compared to 49.6% (λ_{abs1}) and 56.1% (λ_{abs2}) for **P4a**, indicative of the superior electrochromic contrast observed in the case where DalkOTs are substituted with ProDOTs. When fully oxidized, bipolaronic states peaking beyond 1600 nm in the infrared with almost no visible absorption govern their optical spectra, and as a result, both polymers show a remarkably high level of transparency to the human eye.

Figure 4c,d shows the spectroelectrochemical behavior of polymers **P2** and **P5**, the ethynylene-linked derivatives of **P1** and **P4a**. **P2** and **P5** exhibit similar solid-state absorption spectra involving a relatively intense absorption in the UV region and a broad band spanning 450−700 nm due to the dioxythienyl-BTD DA chromophore. Their open gap at about 440 and 450 nm (blue transmission), along with the red transmission between 700 and 800 nm (note especially for **P2**), gives a deep purple hue to these polymers. The overall hypsochromic shift observed when compared to **P1** and **P4a** is a consequence of the insertion of sp-type unsaturated spacers along the DA backbone. However, more significant spectral changes relative to **P1** and **P4a** are evident during oxidation. Examining the depletion of the two absorption maxima, **P2** and **P5** show smaller transmittance changes of 14.3% (λ_{abs1}), 23.3% (λ_{abs2}) and 3.8% (λ_{abs1}), 11.8% (λ_{abs2}), respectively, indicating a limited electrochromic performance. In the case of **P2**, the transition arising in the near-IR (~850 nm) supports the formation of radical cation states which do not ultimately convert into dicationic species, and the long wavelength absorbance beyond 1400 nm is low. Upon further increase of applied potential, **P2** loses its reversible redox activity and the film breaks down. Similarly, **P5** shows a broadly defined pattern in the near-IR involving a polaronic transition and does not result in a well-defined or intense generation of bipolarons. In both cases, the lack of stable bipolaronic states forming on electrochemical oxidation prevents effective bleaching of the UV−vis absorption bands and hinders access to a transmissive doped state. As such, the ethynylene-containing **P2** and **P5** do not address the requirements of a useful system for electrochromic device applications.

Figure 4e,f illustrates the effect of *trans*-ethylene spacers incorporated between the DAD macromonomers on the electrochromicity of the subsequent polymers **P3** and **P6**. As for **P1** and **P4a**, **P3** and **P6** feature a two-band absorption in the visible with a main contribution from the "donor−acceptor" transition. However, in these instances the two transitions have broadened and merged together and now possess a more significant overlap, thus predicting two neutral state polymers of darker tone. While **P3** features a dark blue-green hue in the neutral state, the gradual application of potential first induces the growth of charge carriers in the near-IR with simultaneous depletion of the visible absorption. Considering the two local absorption maxima, **P3** shows substantial transmittance changes of 24.3% (λ_{abs1}) and 50.3% (λ_{abs2}), leading to a clear-gray state upon oxidation. Nonetheless, the redox process is hampered by an irreversible degradation of the active layer as illustrated in Figure 4e (see the final blue curve). From this experimental result, a small potential window of reversible operation is anticipated for this polymer which is undesirable for EC materials (such that further work with this polymer will not be pursued).

As a consequence of the significant bathochromic shift (about 25 nm) and broadening undergone by its short wavelength absorption band, the open gap of polymer **P6** exhibits a local minimum of absorption shifted by 36 nm compared to its parent **P4a**. Likewise, its long wavelength absorption band shifted toward the lower energy region and covers a more extensive bandwidth of the optical spectrum. As a result, **P6** exhibits a saturated green color which is particularly useful in the construction of EC displays. The optically determined energy gap of **P6** (1.50 eV) is slightly narrower than that for **P4a** (1.54 eV). The spectral differences observed between **P6** and **P4a** in their neutral state along with the estimated variation of 0.04 eV in optical bandgaps can be rationalized considering an increase in planarity of the polymer backbone triggered by the introduction of the ethylenic conjugated spacers which minimize the steric interactions between the propylenedioxy bridges of the electron-rich ProDOT units. Upon electrochemical oxidation, **P6** shows excellent transmittance changes of 29.7% (λ_{abs1}) and 37.9% (λ_{abs2}) and switches to a light-gray transmissive doped state. While the transmittance ratios observed are notably lower than the ones measured for **P4a** (49.6% (λ_{abs1}), 56.1% (λ_{abs2})), the relatively uniform bleaching observed across the visible region, along with the formation of stable polaronic and bipolaronic states in the near-IR, projects the potential of this green cathodically coloring polymer for EC applications.

Finally, Figure 4g gives insight into the extent to which the nature of the solubilizing side chains can affect the spectroelectrochemical performance of otherwise identical polymers. In this study, **P4b**, the linear alkyl-substituted DA analogue of **P4a**, shows a transmittance change of 40.3% in the blue region (λ_{abs1}) which is lower by about 9% in comparison with **P4a**. The transmittance change for the long-wavelength absorbance remains high (48.9% (λ_{abs2}) vs 56.1%) in correlation with the near-IR charge-carrier transitions. This variation in contrast can be tentatively rationalized considering an increase of interchain spacing in the case of the branched ethylhexyl-substituted polymer **P4a** compared to the linearly octyl-substituted polymer **P4b** that allows improved ion diffusion and dopant insertion. Overall, **P4a** appears more transmissive than **P4b** in its fully doped state.

Switching Studies. New films of polymer **P1**, **P4a**, **P3**, and **P6** were carefully spray-coated onto ITO, and their deposition was simultaneously monitored by transmittance measurements at their long wavelength absorption maximum (λ_{abs2}). Taking the optical density as representative of the thickness of active layer deposited, polymer thin films of near-identical consistencies were obtained ($\%T(\lambda_{abs2}) = 17-20\%$), allowing reliable comparison of their electrochromic performance. Each film was redox-cycled until a stable and reproducible switch was reached prior to data collection and comparison.

Figure 5 shows the transmittance change (or EC contrast, $\Delta\%T$) attained as a function of time and at the longer wavelength absorption maximum of each material applying square-wave potential steps in the range 10−1 s (ν). In general, square-wave potential stepping experiments are preferred over potential cycling when characterizing the response time of a thin-film electrochrome as significant optical change occurs in less than 0.1 s. In this study, the lower energy transition was chosen to be monitored due to its more intense absorption in the visible region, and it is, in turn, expected that its contrast ratio and rate of depletion will be representative of the polymer's overall EC switching ability.

Parts a and b of Figure 5 compare the response of polymer **P1** and **P4a**, respectively. As predicted by the spectroelectrochemical study, **P4a** exhibits a higher EC contrast (50.6%) at

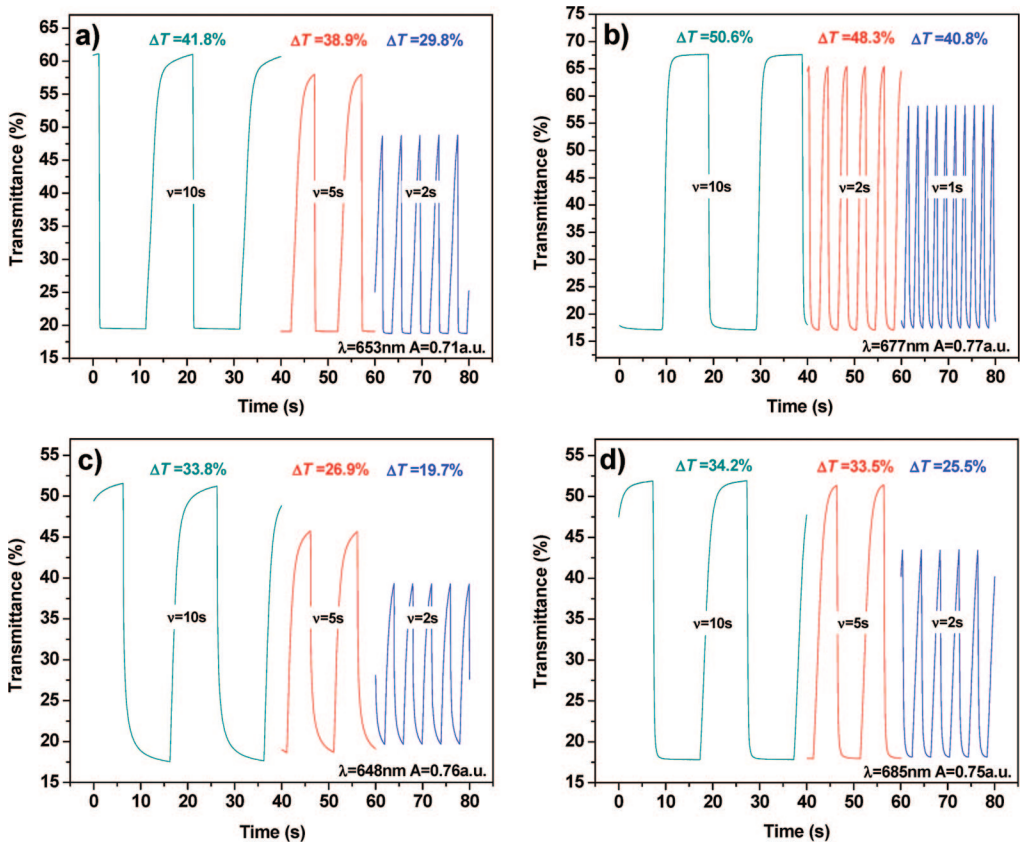

Figure 5. Square-wave potential step absorptometry of spray-coated (a) **P1** (monitored at 653 nm, −0.6 V → +0.65 V vs Fc/Fc^+), (b) **P4a** (monitored at 677 nm, −0.6 V → +0.6 V vs Fc/Fc^+), (c) **P3** (monitored at 648 nm, −0.6 V → +0.6 V vs Fc/Fc^+), and (d) **P6** (monitored at 685 nm, −0.6 V → +0.6 V vs Fc/Fc^+), onto ITO in 0.1 M $LiBF_4$/propylene carbonate solution. Switch times chosen among: 10 s step for 40 s (2 cycles), 5 s step for 20 s (2 cycles), 2 s step for 20 s (5 cycles), and/or 1 s step for 20 s (10 cycles).

the longer wavelength absorption maximum than that of **P1** (41.8%) on slow electrochemical switching ($\nu = 10$ s). As the switch time is decreased from 10 to 2 s, a difference of 29% in the contrast estimated is noted in the case of **P1**, whereas **P4a** undergoes a contrast change of less than 4.5%. It is only by changing the switch time from 10 to 1 s that **P4a** showed a significant loss of contrast, 19% lower in value. Given the similar oxidation potentials, such a notable variation in switching performance between the two polymers can be attributed to the differences in ease of attaining the planar quinoidal geometry characteristic of the oxidized state. With its solubilizing side chains in the plane of the conjugated main chain generally inducing a relative twisting of the polymer backbone, it is likely that **P1** does not possess the same extent of conjugation than **P4a** and is, in turn, not as prone to radical cation (polaron) coupling into stable dications (bipolarons). On the contrary, the ProDOT units of **P4a** exhibit a "spiro-like" center which maintains the branched solubilizing pendant groups out of the plane of the main chain and increases the interchain spacing, allowing ions to penetrate into and out of the film more freely.

Parts c and d of Figure 5 report the response of the two *trans*-ethylene-substituted analogues of **P1** and **P4a**, respectively **P3** and **P6**, to square-wave signals of 10, 5, and 2 s. The EC contrasts of ca. 34% obtained at the longer wavelength absorption maximum on slow switching ($\nu = 10$ s) are in agreement with the spectroelectrochemical estimated values ranging from 35% to 50%. Similar to the parent polymers (**P1** and **P4a**), as the switch time is increased from 10 to 2 s, a decrease of about 42% in the contrasts is noted in the case of **P3**, whereas **P6** undergoes a 2% contrast change from 10 to 5 s and 24% from 5 to 2 s. Overall, in analogy with its control polymer **P4a**, **P6** exhibits higher EC contrasts than **P3** as well as shorter response times. It is worth noting that **P3** was also more sensitive to high oxidation potentials than **P6** and lost its redox reversibility rather rapidly. The difference in switching speed between **P6** and the fully heterocyclic parent **P4a** is tentatively attributed to the decrease of interchain spacing arising from an increase of planarity of the polymer backbone upon insertion of ethylene substituents between the electron-donating building units. It is possible that the reduced interchain spacing hinders the diffusion of the counterbalancing ions from the electrolyte to the active layer. An additional reason could lie in the rotational freedom of the double bond which would inhibit the combination of the radical cationic species.

Colorimetric Measurements. Films of polymer **P1**, **P4a**, **P3**, and **P6** were spray-cast onto ITO-coated glass, and the color changes occurring on redox switching were characterized based on the "Commission Internationale de l'Eclairage" 1976 $L^*a^*b^*$ color standards. Each film was redox-cycled several times, and as shown in Figure 6, the colorimetrically determined relative luminance change, estimating the brightness of the transmitted light as a percentage of the brightness of the light source calibrated to the sensitivity of the human eye, was measured as a function of the doping level induced by electrochemical oxidation (the corresponding absorbance of the films at λ_{abs2} is reported in the legends). Generated using the $L^*a^*b^*$ color coordinates estimated under constant illumination of the polymer thin films, the color swatches shown in Figure 7 give insight into how the structural modifications induced in the DA backbones influence their color states on p-doping. For consistency in comparing the various polymers, the film depositions were here followed by coarse luminance measurements allowing

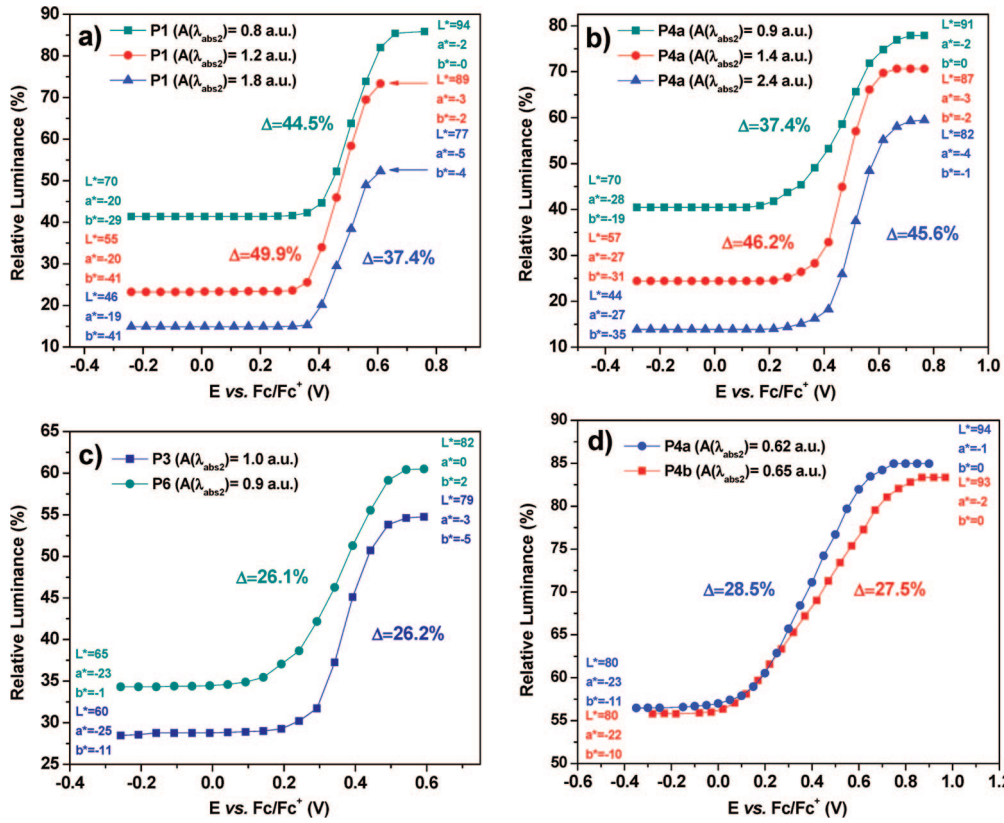

Figure 6. Relative luminance as a function of applied potential and film thickness for spray-coated DA polymers (a) **P1**, (b) **P4a**, (c) **P3** and **P6**, and (d) **P4a** and **P4b**. The legends indicate the absorbance of the deposited films (estimated at the longer wavelength absorption maximum) and give an indication of the thickness obtained on spraying. For color matching, $L^*a^*b^*$ values (in the sense of the Commission Internationale de l'Eclairage 1976 $L^*a^*b^*$ color model) of fully neutral and oxidized states are reported for the films.

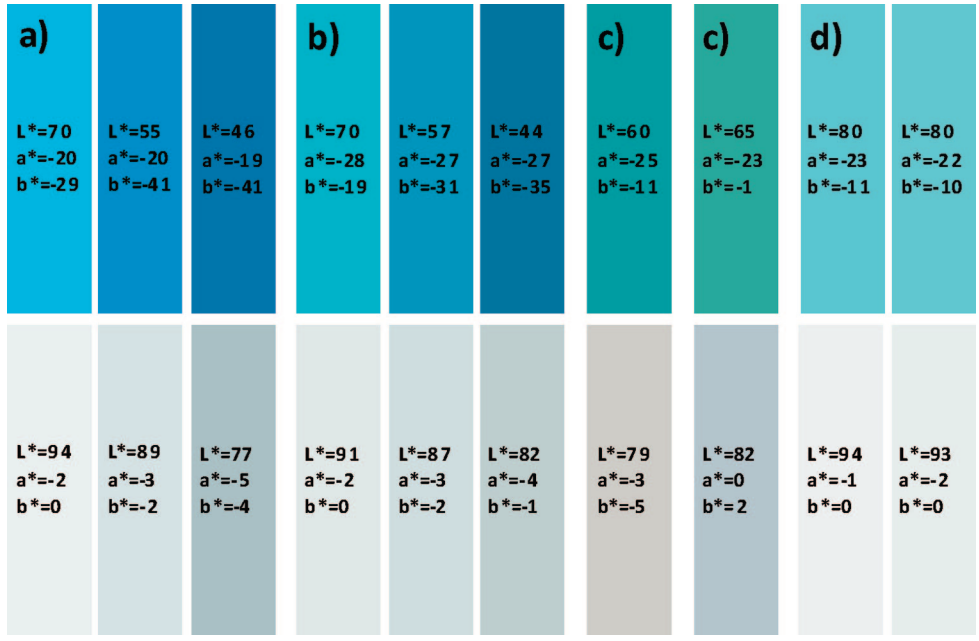

Figure 7. Color matching corresponding to the plots of relative luminance as a function of applied potential and film thickness described in Figure 4 for spray-coated DA polymers (a) **P1**, (b) **P4a**, (c) **P3** and **P6**, and (d) **P4a** and **P4b**. The associated $L^*a^*b^*$ values (in the sense of the Commission Internationale de l'Eclairage 1976 $L^*a^*b^*$ color model) of fully neutral and oxidized states are reported for the films.

to approximately match the polymer optical transmission over the visible.

Parts a and b of Figure 6 compare films of about the same neutral state luminance values of polymers **P1** and **P4a**, respectively. Interestingly, while the monochromatic transmittance ratios estimated by spectroelectrochemical analysis at the local absorption maxima of **P1** and **P4a** predicted slightly higher contrasts in the case of **P4a**, here the colorimetric measures lie in favor of **P1** which, based on the perception of the broad visible region, exhibits luminance-change values as high as ca. 50% and L^* values (ranging from 0 to 100) up to 94, indicative of its aptitude to nearly reach the "white point" of color space.

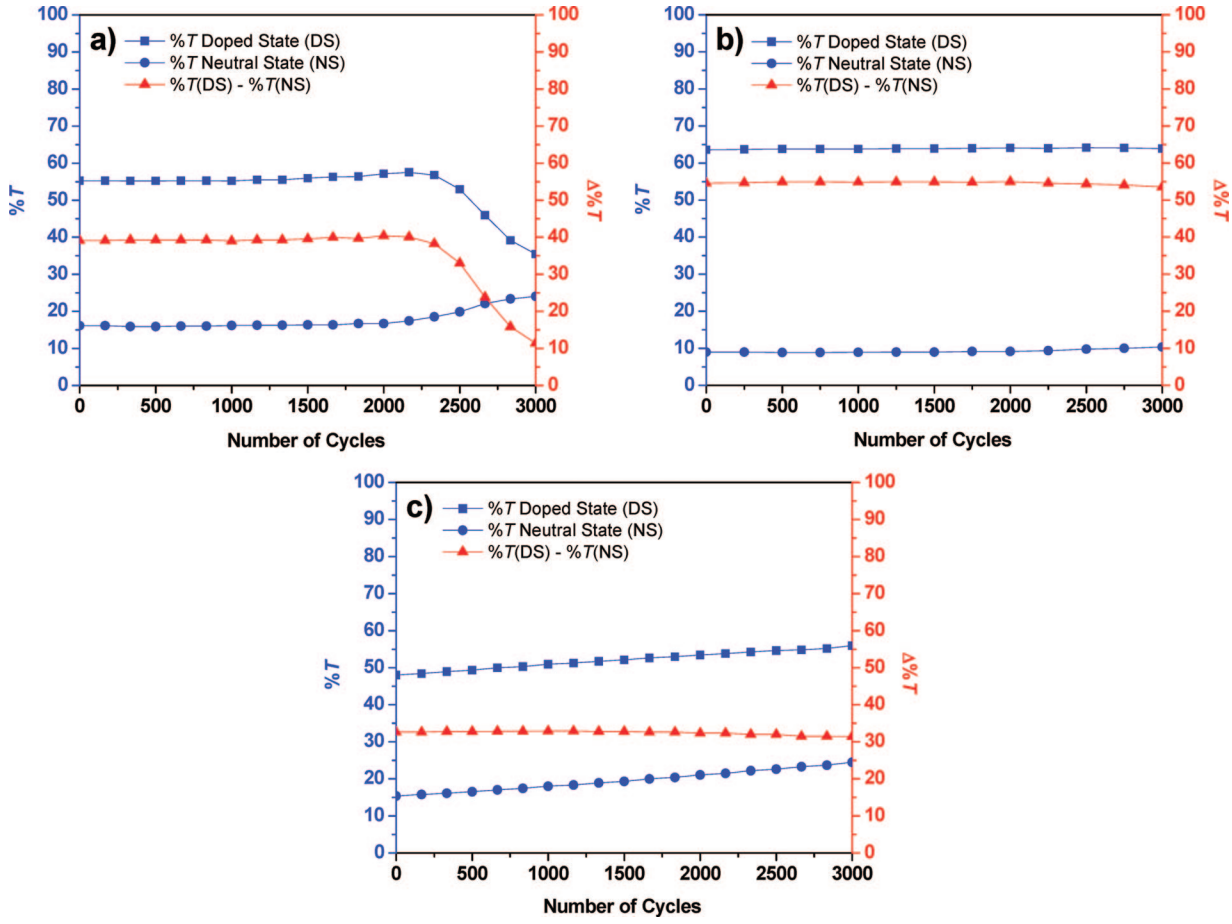

Figure 8. Long-term switching of spray-cast (a) **P1** (monitored at 653 nm, −0.4 V → +0.65 V vs Fc/Fc^+, square-wave potential steps of 4 s, complete cycle is 8 s), (b) **P4a** (monitored at 677 nm, −0.4 V → +0.65 V vs Fc/Fc^+, square-wave potential steps of 6 s, complete cycle is 12 s), and (c) **P6** (monitored at 685 nm, −0.4 V → +0.6 V vs Fc/Fc^+, square-wave potential steps of 6 s, full cycle is 12 s) on ITO in 0.1 M $LiBF_4$/propylene carbonate solution.

Nonetheless, the contrast ratios and transmissivities of **P4a** upon full oxidation remain outstanding as illustrated in Figure 6b. In particular, the luminance change of ca. 45% observed for the thicker deposited film of polymer **P4a** ($A(\lambda_{abs2})$ = 2.4 au) demonstrates exceptional switching characteristics, suggesting good diffusion of the electrolyte through the active layer, in good agreement with the switching performance obtained upon square-wave potential stepping absorptometry (Figure 5b). Overall, both **P1** and **P4a** attain remarkable transparencies with almost no residual hue in their fully oxidized state as indicated by the estimated a^* and b^* values close to those of the clear state of coordinates $a^* = 0$ and $b^* = 0$ (see Figure 7a,b). The large b^* values observed in the neutral state of **P1** account for its deep blue saturation whereas the stronger a^* values obtained for **P4a** justify the green tone of its blue-green neutral state. These two polymers complete their full switch in a potential window of less than 0.4 V.

Figure 6c evaluates how the incorporation of a *trans*-ethylene spacer affects the colorimetric properties of the fully heterocyclic control polymers **P1** and **P4a**. **P3** and **P6** were spray-cast at thicknesses representative of their optimal colorimetric performance. Accordingly, a luminance change of 26% was observed along with little residual hue in the oxidized state as attested by the low a^* and b^* values. Although this luminance change is lower than those observed for the control polymers, such contrasts remain adequate for electrochromic polymers with application in window devices.

A direct effect of the presence of unsaturated spacers regularly inserted in the polymer backbones is the lower b^* values of neutral state **P3** ($b^* = -11$) and **P6** ($b^* = -1$) in comparison with **P1** ($b^* = -41$) and **P4a** ($b^* = -31$) which translates to a progressive loss of blue in their tone with **P6** exhibiting a near-perfect green saturation (see Figure 7c). Similar to **P1** and **P4a**, these two polymers complete their full switch in a potential window of less than 0.4 V.

Figure 6d suggests a slightly sharper color change when branched alkyl solubilizing groups replace the linear ones. At the deposited film thickness ($A(\lambda_{abs2})$ of ca. 0.6 au), the colorimetrically estimated contrasts are near-identical (about 28%), as are the color coordinates of both the neutral and the oxidized states (see Figure 7d). Only a modest improvement in transparency can be observed for **P4a** as predicted by the spectroelectrochemical study. The ease in solution-processing of **P4a** makes this polymer electrochrome stand out when compared to **P4b** and adds advantageously to the moderate optical enhancement observed here.

Stability Studies. Of all the candidates for EC applications synthesized in this study, **P1**, **P4a**, and **P6** stand out in terms of color contrasts, switching times, and short-term redox reversibility as demonstrated throughout the previous sections. To reinforce the potential of these ECPs for integration into ECDs and commercial applications, their long-term switching was investigated on ITO-coated glass applying square-wave potential steps of a duration adapted to the polymers individual response time. Figure 8 demonstrates the performance of the selected polymers as the spray-deposited thin films are subjected to 3000 redox cycles in 0.1 M $LiBF_4$/propylene carbonate solution and under atmospheric conditions.

Measured at its longer wavelength absorption maximum (λ_{abs2} = 653 nm) and using a switching step of 6 s, a transmittance change similar to that monitored in section 3.4.1. ($\Delta\%T(\lambda_{abs2}) \sim 40$) extends with consistency over the first 2000 redox cycles (6 h 40 min) for **P1** as described in Figure 8a. Between 2000 and 2500 cycles, a progressive loss of transparency is observed on doping whereas the film in its neutral state sees only little change in coloration. Such a sudden loss of electrochromicity is a common indication that the contact between the ITO-coated working electrode and the polymer thin-film is altered. In fact, a major difficulty in the synthesis of solution-processable ECPs lies in the trade-off that must be found in the choice of the solubilizing groups considering that the subsequent electroactive polymer thin-film should be sufficiently "insoluble" and compact to remain strongly adhered to the working electrode while being able to swell effectively and allow rapid diffusion of the charge balancing counterions throughout the polymeric network. In the case of **P1**, the combination of the branched nature of the substituents with their in-plane configuration induces an excess of solubility in the context of long-term EC switching. Nonetheless, in devices where gel electrolytes are used, the extent of delamination or dissolution is generally reduced in comparison with a conventional solution electrochemical cell such that it is not always necessary to resynthesize a polymer analogue with shorter solubilizing side chains.

In contrast, **P4a** exhibits a remarkably stable switch over 3000 cycles (10 h based on a 4 s switching step, one cycle is 8 s) as demonstrated in Figure 8b. Measured at its longer wavelength absorption maximum (λ_{abs2} = 677 nm), a variation in electrochromic contrast of only 1% is observed along with no significant loss of transparency in the doped state or color in the neutral state. This outstanding enhancement when compared to **P1** can be attributed to the reduced solubility of **P4a** in solid thin films. The out-of-plane configuration of the solubilizing side chains of **P4a** accounts for an increase of planarity of the conjugated backbone, which in turn affects both inter- and intrachain interactions. This last consideration becomes especially obvious as the somewhat reduced solubility of **P4a** necessitated the use of elevated temperatures to dissolve the polymer rapidly in the casting solvent (toluene) while **P1** dissolves instantaneously at room temperature using the same solvent.

The same long-term stability study (using a 6 s switching step, one cycle is 12 s) performed on the ethylene-unsaturated polymer **P6** revealed a more conventional behavior for an ECP. Thus, as depicted in Figure 8c, a slow but constant variation of transparency in the oxidized state ($\Delta\%T(DS) = 7.9$ after 3000 cycles) and color in the neutral state ($\Delta\%T(NS) = 9.1$ after 3000 cycles) was monitored with increasing number of cycles, whereas the overall transmittance ratio ($\%T(DS)-\%T(NS)$) remains relatively constant during the experiment ($\Delta\%T = 1.2$ after 3000 cycles). As stated previously, this result remains significant considering the nature of the substrate used and the redox induced solubility of the polymer in the solution electrochemical cell as there is little to prevent the chains from slowly migrating toward the platinum counter electrode during the experiment. Nonetheless, this phenomenon could be overcome (at least greatly minimized) by casting the higher molecular weight fraction of **P6**, hence improving both film quality and resistance of the polymer network to repeated switching.

Conclusions

A series of alternating conjugated DA polymeric hybrids containing 3,4-dioxythiophenes, 2,1,3-benzothiadiazole, and unsaturated spacers (either ethynylene or *trans*-ethylene) were synthesized and electrochemically characterized, and their electrochromic performance was evaluated with the goal of attaining a better understanding of the structural requirements to achieving reversibly switching cathodically-coloring ECPs of high contrasts and tunable optical performance. As demonstrated by spectroelectrochemical analysis, the ethynylene-linked DA polymers did not show any useful electrochromicity when compared to their fully polyheterocyclic DA control parents due to the inability to form defined bipolaronic transitions in the near-IR upon electrochemical oxidation. In contrast, the presence of *trans*-ethylene spacers regularly inserted to enhance the coplanarity of the DA polymeric backbones induced narrowing of the energy gaps affording various tones of greens, a color commonly difficult to achieve in the field of π-conjugated polymers. The increased degree of conformational freedom provided allowed stable quinoidal geometries to be formed upon doping and a transmissive oxidized state to be reversibly attained. Further, the more saturated green analogue showed excellent optical and redox stabilities to repeated switching (over 3000 cycles onto ITO) in comparison to its control parent, hence demonstrating the potential of this ECP for device applications.

Beside the fine-tuning of optical properties afforded by the simple structural modifications described in this study, *trans* ethylene-linkers containing ECPs open an obvious pathway toward the synthesis of polymeric electrochromes synthesized via the copolymerization of multiple chromophores. Our group is currently investigating this promising access to new color palettes, including the color black such as desired for electronic ink-based applications.[13,14]

Acknowledgment. We gratefully acknowledge funding of this work by the AFOSR (FA9550-06-1-0192) and DARPA (N00014-06-1-0897).

References and Notes

(1) Havinga, E. E.; Hoeve, W.; Wynberg, H. *Synth. Met.* **1993**, *55*, 299–306.
(2) Kulkarni, A. P.; Tonzola, C. J.; Babel, A.; Jenekhe, S. A. *Chem. Mater.* **2004**, *16*, 4556–4573.
(3) Thompson, B. C.; Fréchet, J. M. J. *Angew. Chem., Int. Ed.* **2008**, *47*, 58–77.
(4) Gunes, S.; Neugebauer, H.; Sariciftci, N. S. *Chem. Rev.* **2007**, *107*, 1324–1338.
(5) Murphy, A. R.; Frechet, J. M. J. *Chem. Rev.* **2007**, *107*, 1066–1096.
(6) Thomas, S. W.; Joly, G. D.; Swager, T. M. *Chem. Rev.* **2007**, *107*, 1339–1386.
(7) Bouffard, J.; Swager, T. M. *Macromolecules* **2008**, *41*, 5559–5562.
(8) Sonmez, G.; Shen, C. K. F.; Rubin, Y.; Wudl, F. *Angew. Chem., Int. Ed.* **2004**, *43*, 1498–1502.
(9) Sonmez, G.; Wudl, F. *J. Mater. Chem.* **2005**, *15*, 20–22.
(10) Reynolds, J. R.; Argun, A. A.; Aubert, P. H.; Thompson, B. C.; Schwendeman, I.; Gaupp, C. L.; Hwang, J.; Pinto, N. J.; Tanner, D. B.; MacDiarmid, A. G. *Chem. Mater.* **2004**, *16*, 4401–4412.
(11) Sonmez, G. *Chem. Commun.* **2005**, 5251–5259.
(12) Monk, P. M. S.; Mortimer, R. J.; Rosseinsky, D. R. *Electrochromism and Electrochromic Devices*; Cambridge University Press: Cambridge, 2007.
(13) Beaujuge, P. M.; Ellinger, S.; Reynolds, J. R. *Nat. Mater.* **2008**, *7*, 795–799.
(14) Krebs, F. C. *Nat. Mater.* **2008**, *7*, 766–767.
(15) Argun, A. A.; Cirpan, A.; Reynolds, J. R. *Adv. Mater.* **2003**, *15*, 1338–1341.
(16) Monk, P. M. S.; Delage, F.; Costa Vieira, S. M. *Electrochim. Acta* **2001**, *46*, 2195–2202.
(17) Corr, D.; Stobie, N.; Bach, U.; Fay, D.; Kinsella, M.; McAtamney, C.; O'Reilly, F.; Rao, S. N. *Solid State Ionics* **2003**, *165*, 315–321.
(18) Sonmez, G.; Sonmez, H. B.; Shen, C. K. F.; Jost, R. W.; Rubin, Y.; Wudl, F. *Macromolecules* **2005**, *38*, 669–675.
(19) Salzner, U. *J. Phys. Chem. B* **2002**, *106*, 9214–9220.
(20) Salzner, U.; Kose, M. E. *J. Phys. Chem. B* **2002**, *106*, 9221–9226.
(21) Durmus, A.; Gunbas, G. E.; Camurlu, P.; Toppare, L. *Chem. Commun.* **2007**, 3246–3248.

(22) Beaujuge, P. M.; Ellinger, S.; Reynolds, J. R. *Adv. Mater.* **2008**, *20*, 2772–2776.
(23) Argun, A. A.; Aubert, P. H.; Thompson, B. C.; Schwendeman, I.; Gaupp, C. L.; Hwang, J.; Pinto, N. J.; Tanner, D. B.; MacDiarmid, A. G.; Reynolds, J. R. *Chem. Mater.* **2004**, *16*, 4401–4412.
(24) Skotheim, T. A.; Reynolds, J. R. *Handbook of Conducting Polymers*, 3rd ed.; CRC Press: Boca Raton, FL, 2007.
(25) Armarego, W. L. F.; Chai, C. L. L. *Purification of Laboratory Chemicals*, 5th ed.; Elsevier: Amsterdam, 2003.
(26) Stille, J. K. *Angew. Chem., Int. Ed.* **1986**, *25*, 508–524.
(27) McCarley, T. D.; Noble, C. O.; DuBois, C. J.; McCarley, R. L. *Macromolecules* **2001**, *34*, 7999–8004.
(28) McCarley, T. D.; McCarley, R. L.; Limbach, P. A. *Anal. Chem.* **1998**, *70*, 4376–4379.
(29) Wyatt, M. F.; Stein, B. K.; Brenton, A. G. *Anal. Chem.* **2006**, *78*, 199–206.
(30) Zhang, X.; Qu, Y.; Bu, L.; Tian, H.; Zhang, J.; Wang, L.; Geng, Y.; Wang, F. *Chem.—Eur. J.* **2007**, *13*, 6238–6248.
(31) Jayakannan, M.; van Dongen, J. L. J.; Janssen, R. A. J. *Macromolecules* **2001**, *34*, 5386–5393.
(32) Montaudo, G.; Montaudo, M. S.; Puglisi, C.; Samperi, F. *Rapid Commun. Mass Spectrom.* **1995**, *9*, 453–460.
(33) Schriemer, D. C.; Li, L. *Anal. Chem.* **1997**, *69*, 4169–4175.
(34) Schriemer, D. C.; Li, L. *Anal. Chem.* **1997**, *69*, 4176–4183.
(35) Axelsson, J.; Scrivener, E.; Haddleton, D. M.; Derrick, P. J. *Macromolecules* **1996**, *29*, 8875–8882.
(36) Thompson, B. C.; Kim, Y. G.; McCarley, T. D.; Reynolds, J. R. *J. Am. Chem. Soc.* **2006**, *128*, 12714–12725.
(37) Hansen, W. N.; Hansen, G. J. *Phys. Rev. A* **1987**, *36*, 1396–1402.
(38) Pavlishchuk, V. V.; Addison, A. W. *Inorg. Chim. Acta* **2000**, *298*, 97–102.
(39) Zotti, G.; Schiavon, G.; Zecchin, S. *Synth. Met.* **1995**, *72*, 275–281.
(40) DuBois, C. J.; Abboud, K. A.; Reynolds, J. R. *J. Phys. Chem. B* **2004**, *108*, 8550–8557.
(41) Yamamoto, T.; Lee, B. L. *Macromolecules* **2002**, *35*, 2993–2999.
(42) Lee, B. L.; Yamamoto, T. *Macromolecules* **1999**, *32*, 1375–1382.
(43) Reeves, B. D.; Grenier, C. R. G.; Argun, A. A.; Cirpan, A.; McCarley, T. D.; Reynolds, J. R. *Macromolecules* **2004**, *37*, 7559–7569.

MA9002787